CHAPTER IV
RESULTS AND DISCUSSION

4.1 Characterization of Organophilic-Clay Filler

4.1.1 FTIR

Typical chemical characteristics of both organic and inorganic materials can be studied by IR spectra analysis. Figure 4.1 shows the FTIR spectra of sodium montmorillonite, dodecylamine and dodecylamine-montmorillonite. Bands at 1050 cm^{-1} associated with Si-O stretching vibrations and between 600-400 associated with Al-O stretching and Si-O bending are the characteristic absorption bands of sodium montmorillonite (Lee and Jang, 1998; Noh *et al.*, 1999; Chen *et al.*, 2000). After treatment with dodecylamine, dodecylamine-montmorillonite exhibits characteristic bands of C-H stretching at 2920 cm^{-1} and 2851 cm^{-1} and C-H bending at 1460 cm^{-1} and 1370 cm^{-1}. The FTIR spectrum of dodecylamine-montmorillonite also shows the specific absorption characteristics of the alumino-silicate layers of montmorillonite. Both dodecylamine and dodecylamine-montmorillonite IR spectra show the absorption peak at 3320 cm^{-1} which is the characteristic of N-H stretching. As seen in the IR spectra of Figure 4.1, all assignments of sodium montmorillonite, dodecylamine and dodecylamine-montmorillonite are summarized in Table 4.1-Table 4.3.

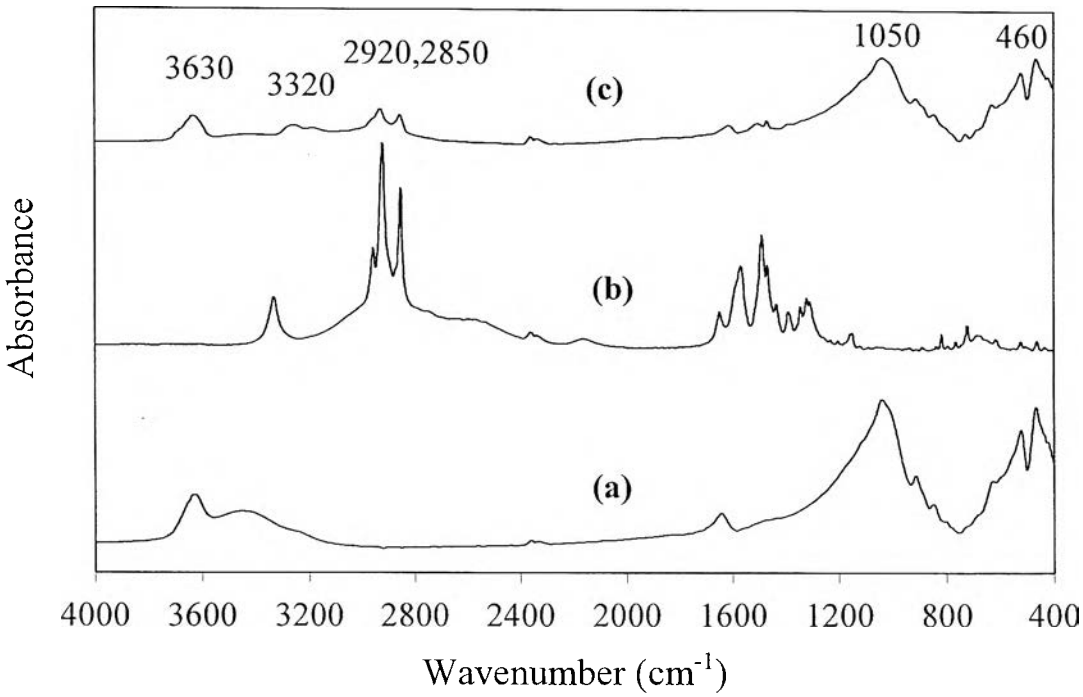

Figure 4.1 The FTIR spectra of (a) sodium-montmorillonite (b) dodeccylamine and (c) dodecylamine-montmorillonite.

Table 4.1 The FTIR absorption bands assignment of sodium montmorillonite.

Frequencies (cm^{-1})	**Assignment**
3630	-OH stretching
3440	-OH stretching (dimers)
1040	Si-O stretching
520	Al-O stretching
460	Si-O bending

Table 4.2 The FTIR absorption bands assignment of dodecylamine.

Frequencies (cm^{-1})	Assignment
3320	N-H stretching of primary amine
2920	C-H stretching of $-CH_2-$ aliphatic chain
2850	C-H stretching of CH_3
1600	Symmetric N-H bending
1460	C-H bending of $-CH_2-$ aliphatic chain
1370	C-H bending of CH_3
1010	C-N stretching in aliphatic amine
720	N-H out of plane bending

Table 4.3 The FTIR absorption bands assignment of dedecylamime-montmorillonite.

Frequencies (cm^{-1})	Assignment
3630	-OH stretching
3440	-OH stretching (dimers)
3320	N-H stretching of primary amine
2920	C-H stretching of $-CH_2-$ aliphatic chain
2850	C-H stretching of CH_3
1600	Symmetric N-H bending
1460	C-H bending of $-CH_2-$ aliphatic chain
1370	C-H bending of CH_3
1050	Si-O stretching
1010	C-N stretching in aliphatic amine
720	N-H out of plane bending
520	Al-O stretching
460	Si-O bending

4.1.2 WAXD

The Wide Angle X-ray Diffraction (WAXD) curves of sodium montmorillonite and dodecylamine-montmorillonite in the region from $2\theta = 2°$ to $10°$ are showed in Figure 4.2 (a) and (b). Each curve has only one peak, at $2\theta = 7.2°$ and $4.9°$ respectively. These peaks are assigned to the 001 lattice spacing of silicate layer in montmorillonite as suggested by Usuki et al. (1993). The lattice spacing corresponds to an interlayer spacing of organophilic montmorillonite. Therefore, the interlayer spacing of sodium montmorillonite and dodecylamine-montmorillonite are 12.17 Å and 17.95 Å. The increment of basal spacing is due to the replacement of inorganic exchange cation by organic cations on the gallery surfaces of smectite clays as described in Figure 4.3 (Okada and Usuki, 1995; Tyan et al.,1999).

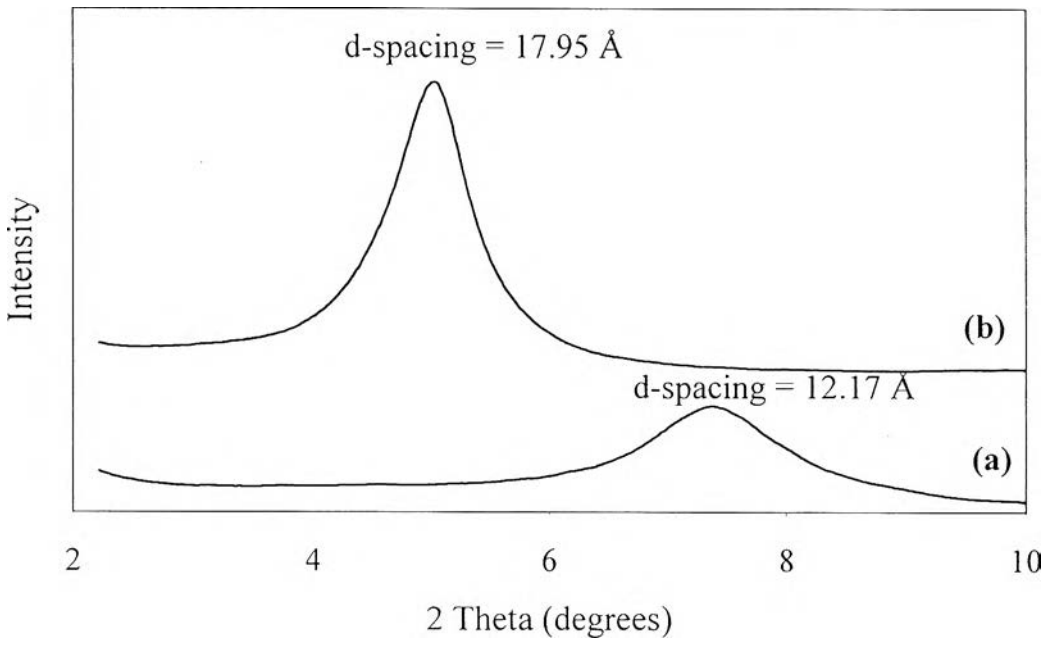

Figure 4.2 The WAXD pattern of (a) sodium montmorillonite and (b) dodecylamine-montmorillonite.

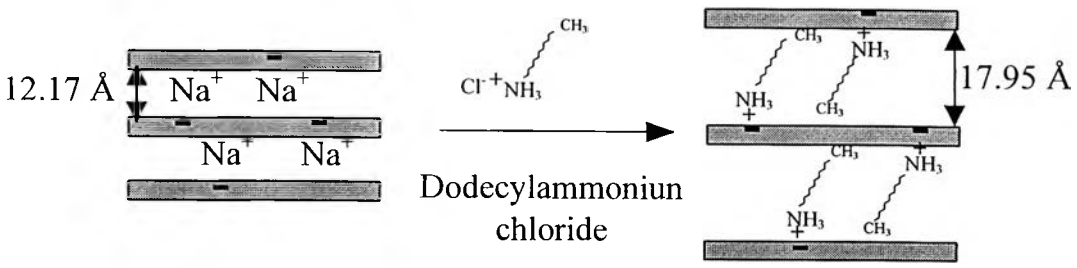

Sodium montmorillonite **Dodecylamine-montmorillonite**

Figure 4.3 Schematic drawing of the replacement of inorganic exchange cation by organic cations.

4.1.3 TGA

TGA thermograms for sodium montmorillonite, dodecylamine, and dodecylamine-montmorillonite are given in Figure 4.4. As evident from the Figure, the onset of sodium montmorillonite decomposition is found at about 655 °C. There is slightly weight loss at 80 °C due to the evaporation of absorbed water in clay. For dodecylamine, the sample shows a dramatic decomposition at temperature of 175 °C, as shown in Figure 4.4 (b). It is observed that the decomposition temperature of dodecylamine-montmorillonite locates at 373 °C between the decompositions of sodium montmorillonite and dodecylamine. This is an indication that dodecylamonium ions react with clay. Furthermore, the thermogram of the dodecylamine-montmorillonite shows the absence of evaporation of absorbed water in the sample at 80 °C.

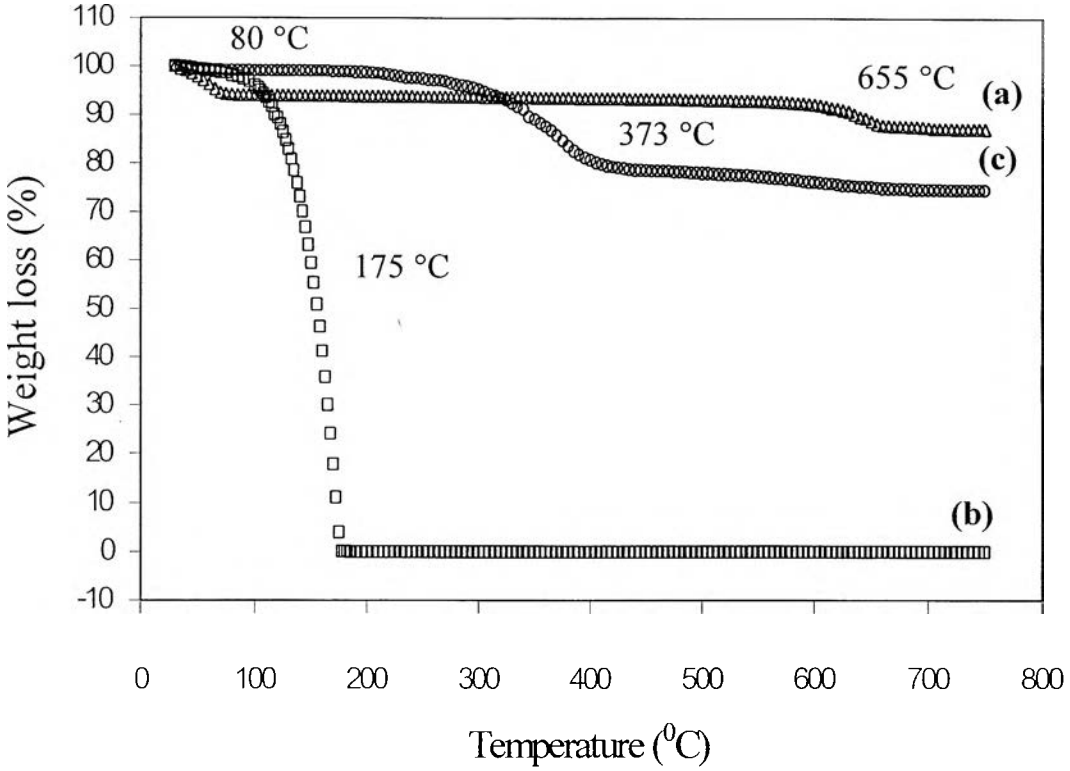

Figure 4.4 TGA thermograms of (a) sodium montmorillonite, (b) dodecylamine, and (c) dodecylamine-montmorillonite.

4.1.4 AAS

The percentage of sodium ions exchange from sodium montmorillonite in the process of preparation of organophilic-clay was determined by air-acetylene flame AAS. From the results, 10 g of sodium montmorillonite which has ion exchange capacity of 119 meq/100 g presented 250 mg of sodium ions. The calculation of percentage Na^+ exchange was calculated by using equation 4.1,

$$\textbf{\% Na}^+ \textbf{ Exchange} = \frac{\textbf{Amount of Actual Na}^+}{\textbf{Amount of Theoritrical Na}^+} \times \textbf{100\%} \qquad (4.1)$$

Consequently, the percentage of sodium ions exchange is equal to 91.34% (see the calculation in Appendix II).

4.2 Characterization of Polyimide-Clay Nanocomposite Thin Films

4.2.1 FTIR

The IR spectra of the representative composition are illustrated in Figure 4.5 along with those of dedecylamine-montmorillonite (Do-MMT), polyimide (PI), and polyimide-montmorillonite (PI-MMT). It is clearly seen that the spectra of the composites exhibit the presence of characteristic absorption due to both the organic and inorganic groups. The absorption bands at 3630, 2920, 1050, and those between 600-400 cm^{-1} can be associated respectively with –OH stretching of the lattice water, C-H stretching, Si-O stretching, and Al-O stretching in Do-MMT. For polyimide demonstrated in spectrum (b), it shows clear appearance of the bands at 1778 and 1726 cm^{-1}, which are characteristic of carbonyl group (C=O) stretching in imide groups, and the band at 1374 cm^{-1}, which is characteristic of C-N stretching in imide groups as described by Li *et al.* (1998). Spectrum (c) is from the PI-MMT nanocomposite film which demonstrated both characteristic peaks of Do-MMT and PI.

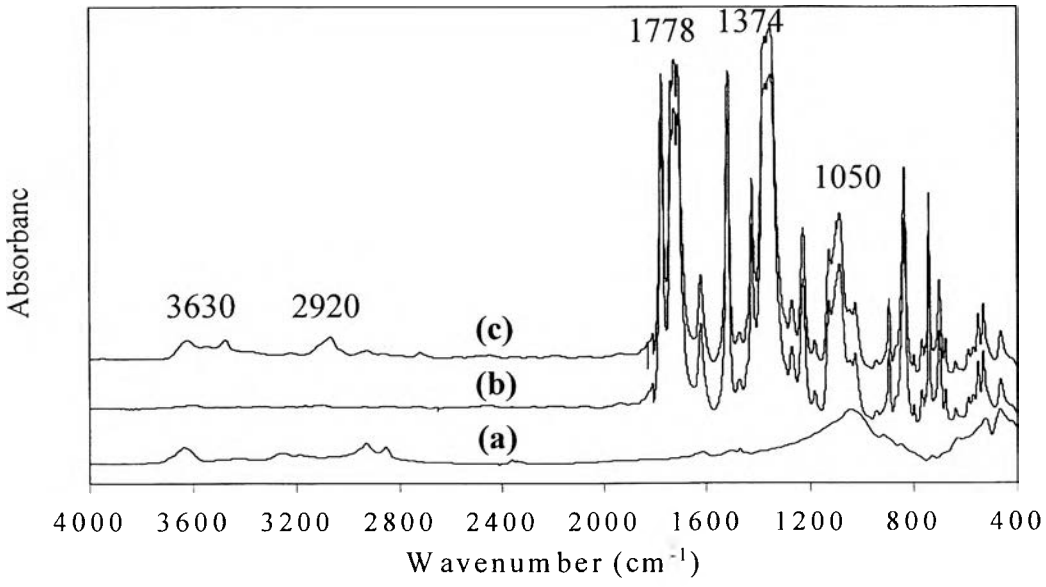

Figure 4.5 FTIR spectra of (a) dodecylamine-montmorillonite, (b) polyimide, and (c) polyimide-montmorillonite.

4.2.2 WAXD

Figure 4.6 shows X-ray diffraction curves of polyimide and polyimide-montmorillonite (3 wt% clay). In the case of PI-MMT (3 wt% clay), the curve shows no peak, that means the peak corresponding to the basal spacing has disappeared. This fact reveals that organophilic-clay in nanocomposite material disperses homogeneously into the polyimide matrix (Pinnavaia, 1996). Therefore, polyimide-clay nanocomposite at 3 wt% can be classified as an exfoliated nanocomposite as shown by WAXD and TEM results in Figure 4.7. The broad band in the region between 2θ = 12°-30° suggests that the films contain amorphous regions or partially order structures.

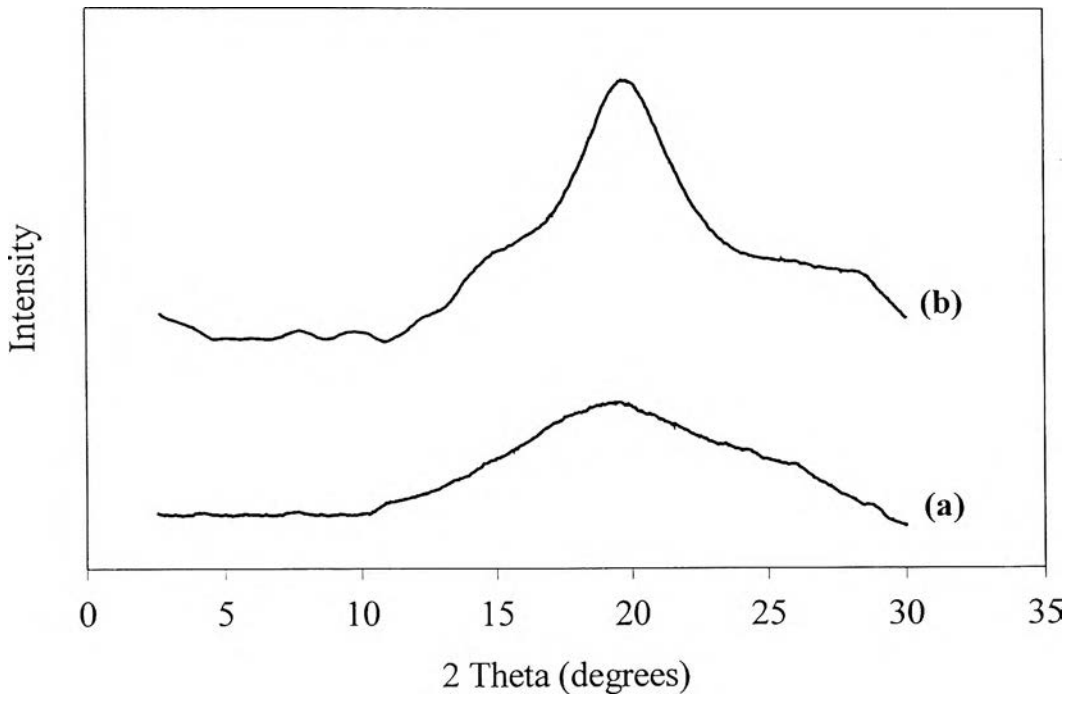

Figure 4.6 WAXD patterns of (a) polyimide and (b) polyimide-montmorillonite.

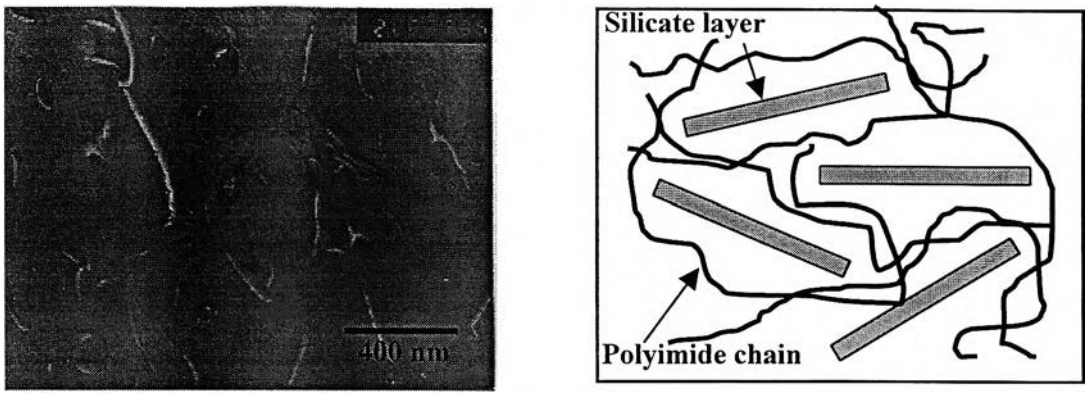

(a) (b)

Figure 4.7 (a) TEM of polyimide-clay nanocomposite film (3 wt% of clay) and (b) schematic of exfoliated nanocomposite (Lilayuthalert, 1998).

4.2.3 TGA

TGA curves of polyimide and polyimide-clay nanocomposite are illustrated in Figure 4.8. The decomposition temperatures of PI and PI-clay are 585 °C and 625 °C, respectively. As evident from the Figure, the onset of polyimide matrix decomposition in the nanocomposite is found to move to higher temperature, indicating the enhancement of thermal stability of composite. This should result from the hydrophobic interaction between the polyimide chain and alumino-silicate layer of filler. An additional amount of thermal energy is probably needed to destroy this specific interaction, so the inorganic filler can delay the thermal degradation of the polymeric material.

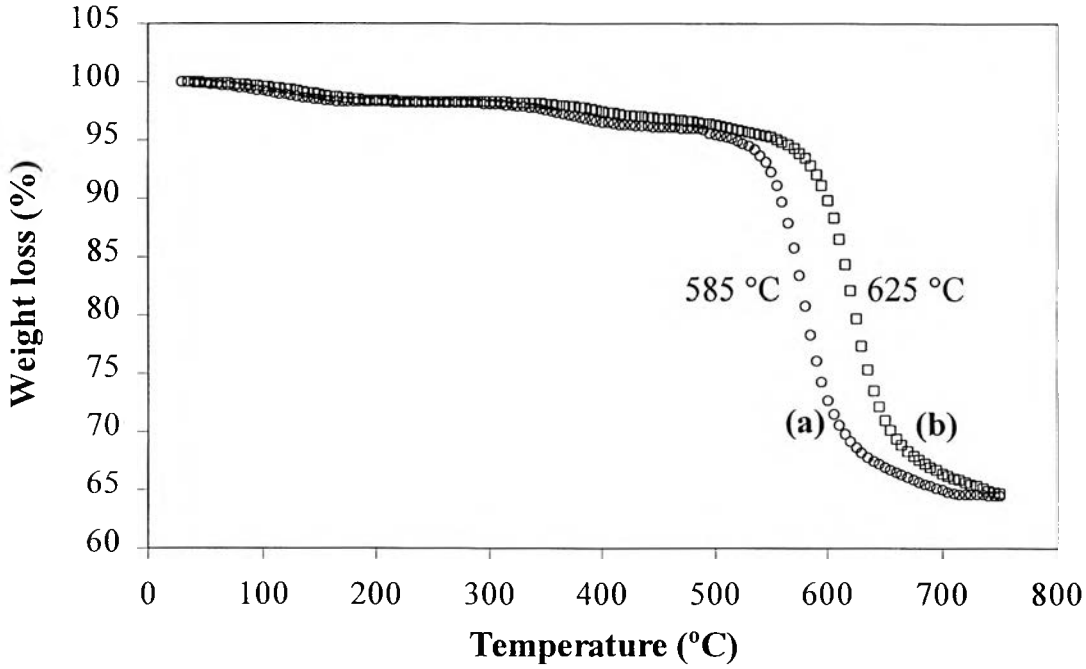

Figure 4.8 TGA thermograms of (a) polyimide film and (b) polyimide-clay film (3 wt% clay).

4.3 Property Measurement

4.3.1 Gas Permeability

As a protective coating for gas sensor, a polymer should have a low level of gas permeability to avoid any characteristic change of gas sensor. Figure 4.9 shows the O_2 gas permeability of PI, PI-clay (3%), and PI-clay (6%) with various thickness of 15, 25, and 35 μm (see Appendix III). The polyimide-clay nanocomposite was found to be superior in its gas barrier property to ordinary polyimide. Furthermore, the dependence of montmorillonite content on O_2 gas permeability was also investigated. The results show that the higher content of clay, the lower O_2 gas permeability. The big decrease of the gas permeability is explained by the increase of the total path of the gas (Yano *et al*, 1993; Giannelis, 1996). As shown by TEM, montmorillonite is disposed parallel to the film surface. In this case, the total

path of diffusing gas increases. Figure 4.10 shows a conceptual picture of the path of diffusing gas through the polyimide-clay hybrid as described by Yano *et al.* (1993, 1997). For the various values of thickness, the gas permeability decreases with increasing thickness and shows the same trend with increment of clay content. Only 3 wt% addition of montmorillonite brings gas permeability value to be less than half of the value of polyimide.

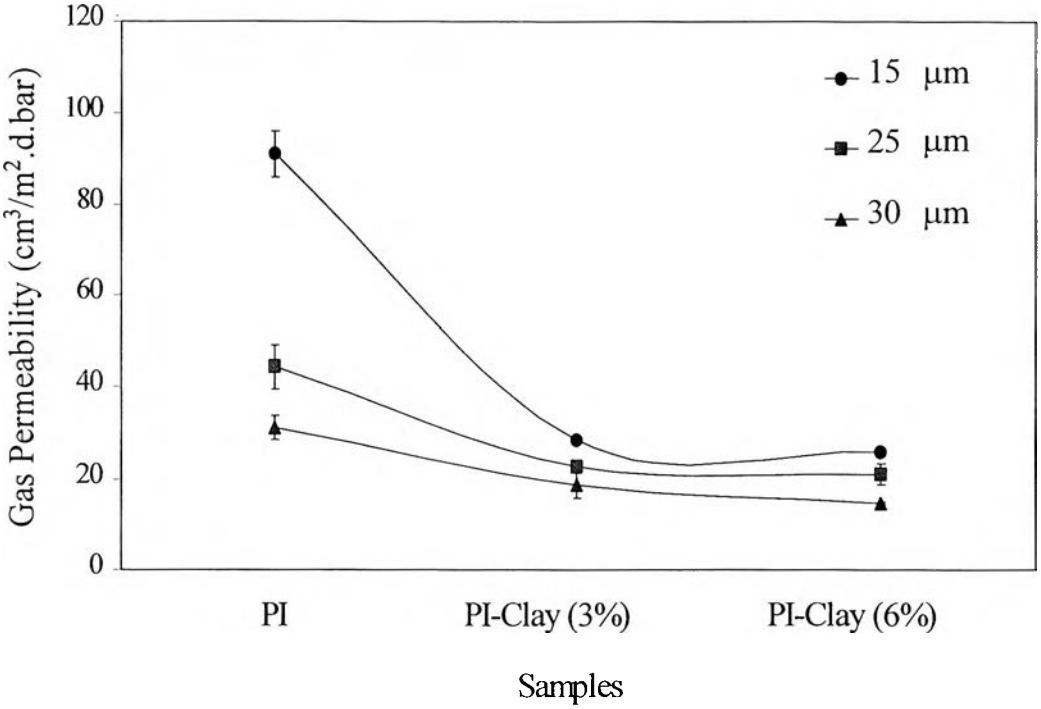

Figure 4.9 Montmorillonite content and film thickness dependence of O_2 gas permeability of polyimide-clay hybrid.

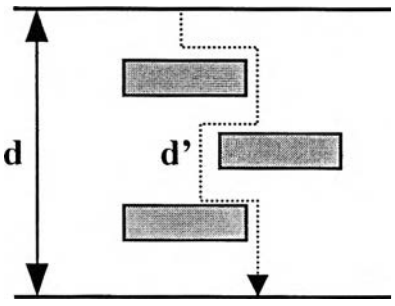

d : thickness of a film
d' : tortuosity path of a diffusing gas

Figure 4.10 A model for the path of diffusing gas through the polyimide-clay hybrid.

4.3.2 Electrical Resistivity

As a protective coating for microelectronic gas sensor applications, the plastic electrical resistivity is of functional significance. Figure 4.11 shows the electrical resistivity of polyimide and polyimide-clay hybrid with various clay contents (see Appendix IV). It is found that higher loading of clay contents raises the electrical resistivity of the films at the temperature range of 50-350 °C. This evidence can be explained by the prevention of intermolecular charge transfer of polyimide chain. Dense packing is necessary for formation of the order structures required for intermolecular charge transfer. Therefore, in polyimide-clay hybrid, clay acts as hindrance which reduces the possibility for polymer chain to form well-packed donor/acceptor pairs. Moreover, it has been observed that electrical treeing can be inhibited by the presence of certain finely divided inorganic fillers (Ku and Liepins, 1987). That means the increment of electrical resistivity is caused by the inhibition of electrical tree by clay particles.

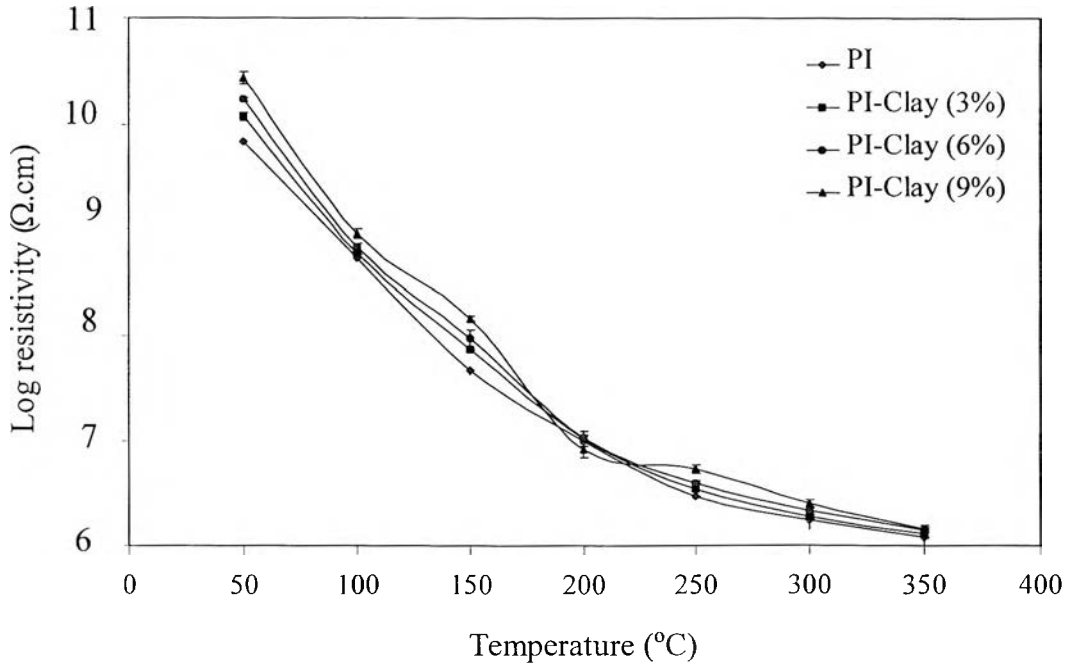

Figure 4.11 Electrical resistivity measurement of polimide-clay hybrid.

The dependence of temperature on electrical resistivity is also shown in Figure 4.11. As temperature increases by the step of 50 °C, the electrical resistivity of the films decreases remarkably. At the highest temperature, 350 °C, the electrical resistivity drops from the order of 10^{10} Ω.cm to 10^{6} Ω.cm, which is still in the range of electrical resistivity for insulation class, as showed in Table 4.4. The decline of electrical resistivity can be described by energy band as illustrated in Figure 4.12. In the ground state of insulator, all bands are either completely filled (the valence band) or completely empty (the conduction band). The highest energy electrons in the ground state must gain additional energy, E_g, before they can reach empty orbitals and become mobile, so that electrical conduction can occur. At absolute zero degree temperature, any material with an energy gap is nonconducting. However, at any finite temperature, there is a probability that some electrons will be thermally excited across the energy gap into the lowest unoccupied molecular orbital band (the conduction band), leaving behind unoccupied positive holes in the valence band. Since the electrons in the bottom of the conduction band and the positive hole in the top of the valence band are in the same molecular orbital that extend throughout the entired material, both can contribute to the conduction process leading to reduction of electrical resistivity.

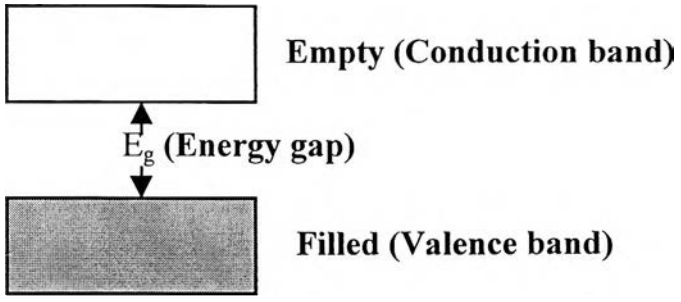

Figure 4.12 Energy bands in an insulator.

Table 4.4 Classification of materials based on electrical resistivity.

Resistivity (Ω.cm)	Class
$0\text{-}10^3$	Conductor
$10^3\text{-}10^7$	Partial conductor or semiconductor
$10^5\text{-}10^{18}$ and higher	Insulator

4.3.3 Adhesion

In the microelectronics field, the adhesion improvement with γ-amino propyltriethoxysilane (γ-APS) is due to the chemical interaction of the silane with silicon substrate (SiO_2) surface and with PI matrix. Therefore, in order to understand adhesion at these interfaces, it is important to know what group of the γ-APS bond with the substrate, and which ones are available for bonding with PI precursor. Figure 4.13 demonstrates the chemical structure of γ-APS, hydrolysis and its bonds with the substrate and polyimide matrix. The γ-APS molecule bonds to the substrate via covalent bond formation and forms an interpenetrating network with polymer matrix (Ghosh and Mittal, 1996). The covalent bond has high bond energy (70-800 kJ/mol) and is the desired interfacial interaction leading to a reliable bond.

Figure 4.14 shows shear strength between polyimide-clay hybrid and silicon wafer (see Appendix V). The higher clay content brings shear strength to value more than that of original unfilled polyimide. Since γ-APS was applied between PI-clay and silicon wafer, ionic interaction of amonium group (NH_3^+) at γ-APS chain end can occur with negative charges normally generated on the surface of silicate layer of clay as shown in Figure 4.15. Since the ionic bond (electrostatic interaction) also has high bond energy (160-600 kJ/mol) relative to that of covalent bond, the higher clay content can bring about the increment of shear strength.

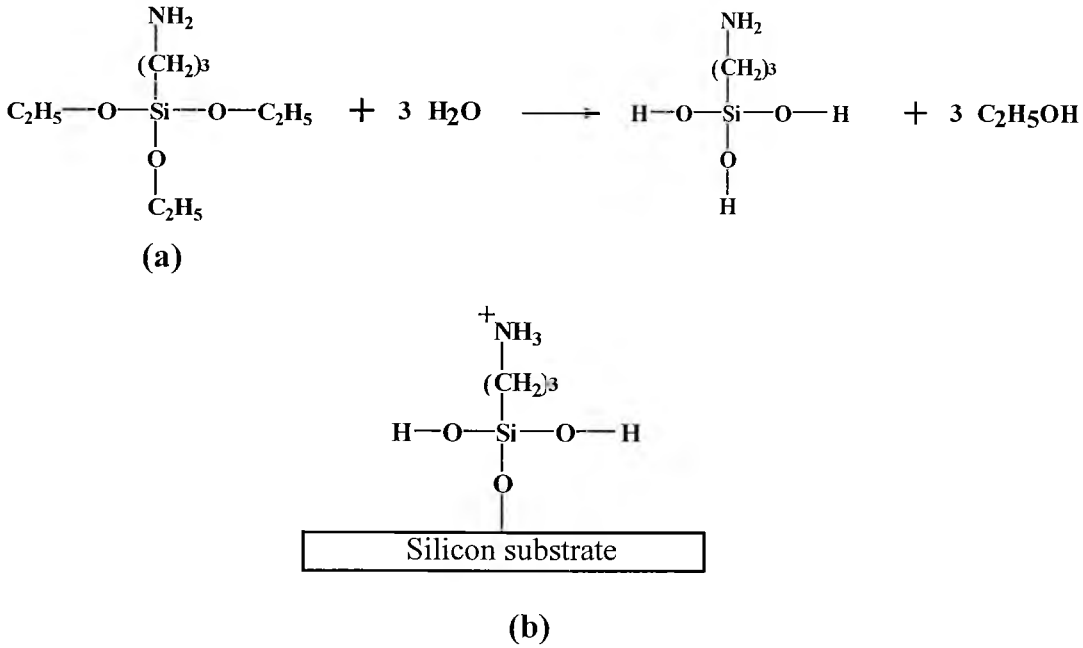

Figure 4.13 (a) The chemical structure of γ-APS and hydrolysis reaction and (b) its bonds with the substrate and polyimide matrix.

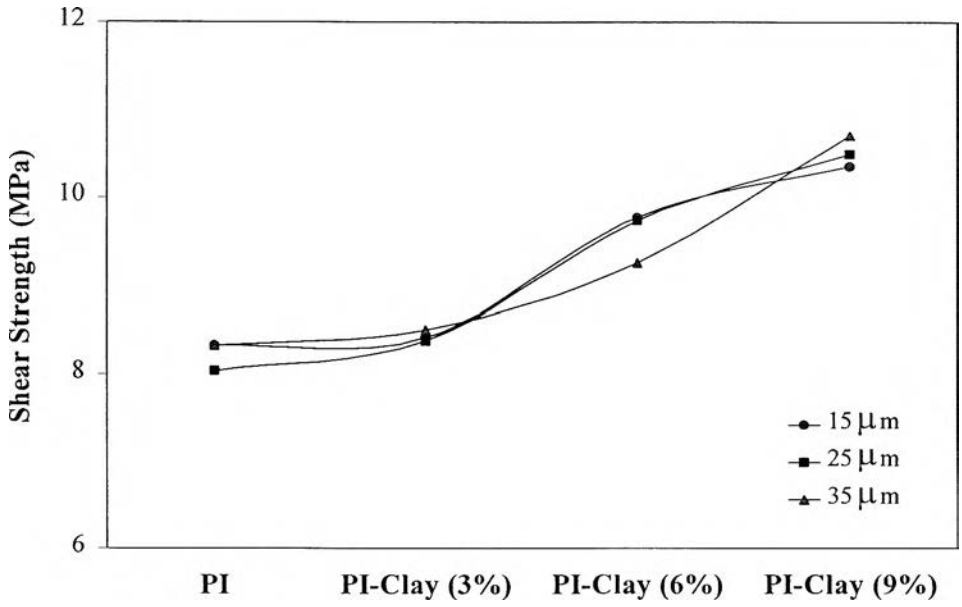

Figure 4.14 Shear strength between polyimide-clay hybrid and silicon wafer.

Moreover, the result shows that thickness has no effect on adhesion between the films and silicon substrate because a prerequisite for the chemical interaction is the closeness of the active site across the interface. Interaction between active sites will become unimportant when the distance between the reacting groups is in the excess of 0.5 nm (Ghosh and Mittal, 1996).

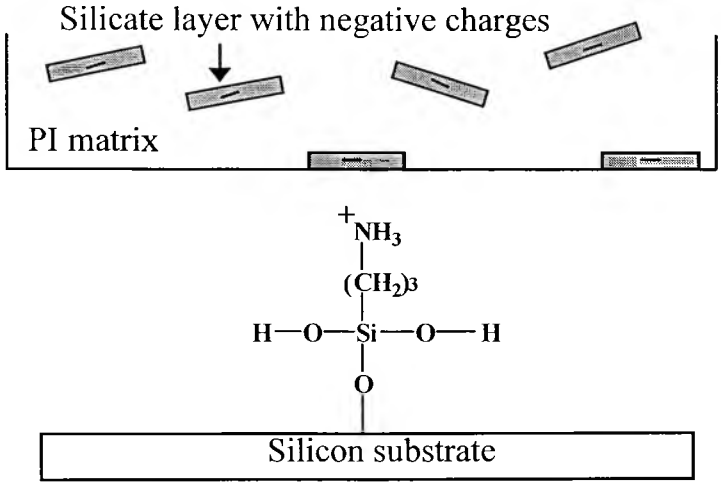

Figure 4.15 Ionic bond between γ-APS and silicate layer.

To make sure that an adhesive failure occurs at the interface between thin film and silicon substrate, not cohesive failure, optical microscope was used to examine the surface at break. Figure 4.16 shows the surfaces of the film and silicon substrate after pulling by Instron universal testing machine. It is found that both surfaces are smooth, so the adhesive failure occurs.

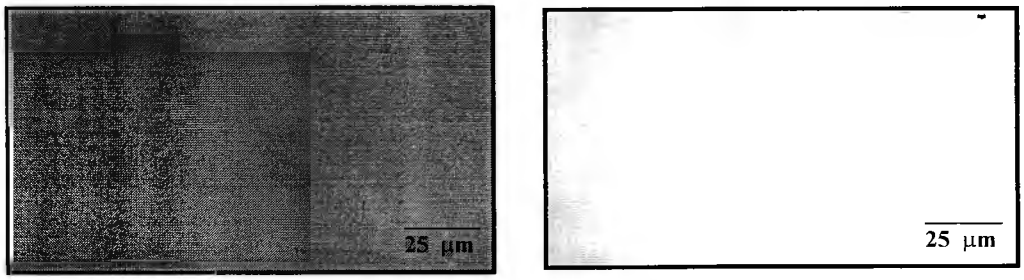

(a) **(b)**

Figure 4.16 Surfaces of (a) polyimide-clay film and (b) silicon wafer after break.